Geoscience Frontiers 11 (2020) 1681–1693

Contents lists available at ScienceDirect

Geoscience Frontiers

journal homepage: www.elsevier.com/locate/gsf

Research Paper

New discriminant-function-based multidimensional discrimination of mid-ocean ridge and oceanic plateau

Surendra P. Verma [a,*], Lorena Díaz-González [b]

[a] Instituto de Energías Renovables, Universidad Nacional Autónoma de México, Priv. Xochicalco S/no., Col. Centro, Apartado Postal 34, Temixco, Mor, 62580, Mexico
[b] Centro de Investigación en Ciencias, Universidad Autónoma de Estado de Morelos, Cuernavaca, Morelos, 62209, Mexico

ARTICLE INFO

Handling Editor: Richard Palin

Keywords:
MORB
Multivariate discordant outliers
Log-ratio transformation
Multidimensional discrimination
Analytical uncertainties
Post-emplacement changes

ABSTRACT

From a compilation of geochemical data for the discrimination of the tectonic settings of mid-ocean ridge (MOR; 3730 samples) and oceanic plateau (OP; 3656 samples), we present two new discriminant functions and diagrams obtained from censored multivariate discordant outlier-free datasets. Ten different sets of data (original concentrations as well as isometric log-ratio transformed (ilr) variables; all 10 major (M) elements as well as all 10 major and 6 trace elements MT) were used to evaluate the quality of discrimination from linear discriminant analysis (LDA) and canonical analysis. Two selected multidimensional models ilr_M (9 ilr transformed variables of multi-normally distributed 10 major elements) and ilr_{MT} (15 ilr transformed variables of multi-normally distributed combined 10 major and 6 trace elements), considered as the best or most representative (total of 5650 samples for ilr_M and 2858 for ilr_{MT}), provided percent success values, respectively, of 80.9% for the MOR and 81.1% for the OP (ilr_M) and 88.5% for the MOR and 90.1% for the OP (ilr_{MT}). Both processes (log-ratio transformation and multi-normality) rendered the percent success values similar for both groups (MOR and OP). The respective discriminant functions were successfully used for four tests from known tectonic settings and four application cases (two for ophiolites and two for Precambrian rocks), documenting thus the utility of the new discrimination procedure for the MOR and OP tectonic settings. Furthermore, we showed that our multidimensional procedure is robust against analytical errors or uncertainties, as well as post-emplacement compositional changes caused by element mobility from both low or high temperature alteration. The robustness against the gain or loss of a single element at a time was also documented, from which the ilr_{MT} model was evaluated as more robust than the ilr_M model. A new online computer program MOROPdisc was written in Java Framework ZK, which is freely available for use at our web portal http://tlaloc.ier.unam.mx.

1. Introduction

The geochemical tools of discrimination diagrams (e.g., Pearce and Cann, 1971, 1973; Wood, 1980; Shervais, 1982; Agrawal et al., 2008; Verma et al., 2015; Verma and Armstrong-Altrin, 2016; Verma, 2020) have been in use now for over 45 years with thousands of literature references. Although older bivariate and ternary diagrams have been evaluated less successful for tectonomagmatic discrimination, the newer multidimensional diagrams have been shown to work efficiently (Verma, 2010, 2015, 2020).

The multiple reasons why the multidimensional approach based on log-ratio transformation and linear discriminant and canonical analysis works well, in fact, much better than the conventional bivariate and ternary diagrams, are as follows (Verma, 2020): (i) the advantages of two or three elements at a time are added or enhanced in multidimensions; (ii) the element concentrations have a less discriminating power than their ratios; (iii) the element ratios are less prone to post-emplacement changes than the element concentrations; (iv) the element concentrations are more dependent on the degree of partial melting, fractional crystallization and other petrogenetic processes than the element ratios, the latter depend on the relative values of solid/liquid partition coefficients (e.g., Rollinson, 1993); (v) probability-based decisions can be achieved in the multidimensional approach when combined with linear discriminant and canonical analysis (Agrawal, 1999); (vi) the geochemical elements are characterised by problems of closure and constant sum, which are overcome by log-ratio transformations (Aitchison, 1986;

* Corresponding author.
E-mail addresses: spv@ier.unam.mx (S.P. Verma), ldg@uaem.mx (L. Díaz-González).
Peer-review under responsibility of China University of Geosciences (Beijing).

https://doi.org/10.1016/j.gsf.2020.01.005
Received 15 August 2019; Received in revised form 24 October 2019; Accepted 2 January 2020
Available online 22 January 2020

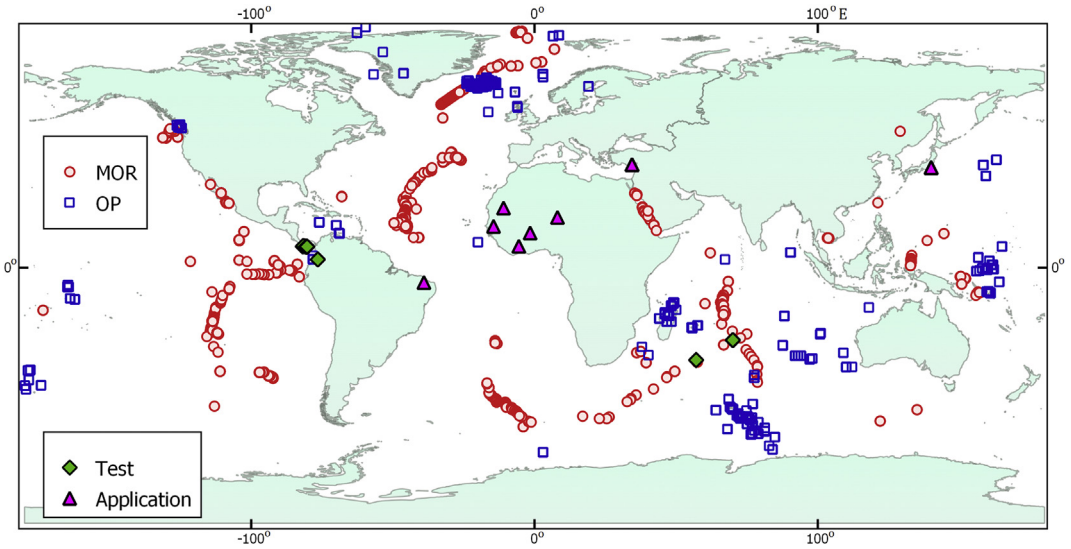

Fig. 1. Schematic location map of the MOR and OP database and test and application studies.

Egozcue et al., 2003; Verma, 2012); (vii) the error distortion, amplification and reduction documented for ternary diagrams can be fully eliminated in the multidimensional approach (Verma, 2012, 2015); and (viii) the computer programs available at the web portal http://tlaloc.ier.unam.mx facilitate the application of the multidimensional solution.

The multidimensional approach (Verma and Armstrong-Altrin, 2013, 2016) has already been widely adopted for the study of sedimentary rocks, along with the recommendation that the conventional diagrams may be abandoned (Armstrong-Altrin and Verma, 2005), although it is yet to happen in the study of igneous rocks. Nevertheless, we also need multidimensional solutions to problems not yet fully addressed from the conventional diagrams.

Thus, despite the wide use of tectonomagmatic discrimination tools, no multidimensional diagrams are yet available for the discrimination of mid-ocean ridge (MOR) and oceanic plateau (OP) settings, except a preliminary diagram proposed relatively recently by Verma et al. (2015) and a conventional diagram of Condie (2001) with eye-drawn boundaries. Both MOR and OP settings seem to be important sites of oceanic volcanism (e.g., Schilling et al., 1983; Le Roex, 1987; Mahoney et al., 1995; Kerr et al., 1996; Tejada et al., 2002; Serrano et al., 2011; Yi et al., 2014). Yet, even in the recent study of ophiolites (Furnes and Safonova, 2019), "oceanic plateau" was mentioned only at one place and the OP was not discriminated from the MOR setting. Similarly, in the study of ophiolites, Saccani (2015) was unable to distinguish the OP from the MOR setting.

One may argue that, because it would not be possible to subduct an oceanic plateau, there is no need to discriminate this tectonic setting from the MORB. It may not be true for at least four reasons as follows: (i) a thick crust of submarine ridges can be subducted beneath continents, such as the Cocos Ridge being subducted beneath Central America (e.g., Johnston and Thorkelson, 1997); (ii) in the oceanic plates, there are probably no older OP than the Cretaceous (Where are the older OP?); (iii) on land (Furnes and Safonova, 2019), there are also OPs (Were they formed on continents? If so, why are they called OP?); and (iv) the OP setting was identified for Neoproterozoic terranes of the Punagarh area of the Aravalli craton by Verma et al. (2015) from sequential testing in discrimination diagrams. To answer at least some of these questions, we need to develop efficient tools to discriminate the OP from the MOR setting and apply them to the study of ophiolites and older terranes.

From a limited database of 798 and 176 samples for the MOR and OP, respectively, Verma et al. (2015) used the additive log-ratio transformation (Aitchison, 1986) of major elements to propose a discriminant function from the linear discriminant analysis (LDA) and canonical analysis. Verma et al. (2015) did not use the combination of major and trace elements for the MOR-OP discrimination, which, from intuition, may be more efficient because of higher dimensions than only the major elements and probably higher discrimination power of trace elements as compared to most major elements. However, the role of the dimensionality of the solution on the percent success or correct classification of such discrimination diagrams has still not been fully documented, although some indications are available on the increase of percent success with increase of dimensions (Verma and Armstrong-Altrin, 2016; Verma, 2020).

Therefore, discriminant functions from major as well as combination of major and trace elements of a more representative database of the MOR and OP settings are still much needed, being the main objective of this study. We also focus on clearly documenting the effect of the number of dimensions in the solution of tectonic discrimination as well as testing and applying the multidimensional solution and evaluating its robustness against post-emplacement changes and analytical uncertainties.

2. Procedure for proposing multidimensional discrimination

A worldwide database was established for both tectonic settings (MOR and OP; Fig. 1) from numerous references listed in the Supplementary File. All data were processed in IgRoCS (Verma and Rivera-Gómez, 2013), under the Middlemost (1989) option for Fe-oxidation adjustment, to assign magma and rock types to each sample. In summary, MOR was initially represented by 3730 (21 ultrabasic, 3394 basic, 227 intermediate, and 88 acid magma) samples and OP by 3656 (133 ultrabasic, 3001 basic, 392 intermediate, and 130 acid) samples. All samples, irrespective of their magma types, were used in the tectonic discrimination (Table 1).

For the major element-based discrimination, although 100% adjusted volatile-free major element data are provided by IgRoCS, these data have the two Fe-oxidation states split as Fe_2O_3 and FeO in different proportions, as suggested by Middlemost (1989) for different rock and magma types. Because we are considering all rock and magma types together, we decided to use a different 100% adjustment by keeping total Fe as $Fe_2O_3^t$. In other words, we used the major element data as 10 oxides (instead of 11) adjusted to sum up to 100% on an anhydrous basis. This should be a common practice to avoid the effects of Fe oxidation in the multidimensional solution.

The adjusted major element concentration data were used for the LDA and canonical analysis. All 10 elements in combination did not provide a solution, because the most abundant element SiO_2 was not significantly

Table 1
Discrimination of mid-ocean ridge (MOR) and oceanic plateau (OP) tectonic settings.

Item No.	Dimensions and discriminating variables		Number of samples used (%)			Number and % of correctly discriminated samples						Number and % of incorrectly discriminated samples	
	No.	Name	MOR	OP	Total	MOR		OP		Total		Number	%
			Number	Number	Number	Number	%	Number	%	Number	%		
1	9	TiO_2 to P_2O_5 (M) all	3730	3656	7386	3052	81.82	2531	69.23	5583	75.59	1803	24.41
2	9	TiO_2 to P_2O_5 (M) multinormal	2558	1839	4397	2027	79.24	1524	82.87	3551	80.76	846	19.24
3	9	ilr major (M) all	3730	3656	7386	2767	74.18	2754	75.33	5521	74.75	1865	25.25
4	9	**ilr major (M) multinormal***	**2788**	**2862**	**5650**	2255	**80.88**	2321	**81.10**	4576	**80.99**	1074	**19.01**
5	14	TiO_2 to P_2O_5 (no MnO), 6 trace (MT) all	1564	2322	3886	1408	90.03	1852	79.76	3260	83.89	626	16.11
6	14	TiO_2 to P_2O_5 (no MnO), 6 trace (MT) multinormal	657	966	1623	621	94.5	871	90.2	1492	91.9	131	8.1
7	15	ilr major trace (MT) all	1564	2321	3885	1266	80.95	2015	86.82	3281	84.45	604	15.55
8	15	**ilr major trace (MT) multinormal***	**1126**	**1732**	**2858**	966	**88.45**	1561	**90.13**	2557	**89.47**	301	**10.53**
9	9	TiO_2 to P_2O_5 (M) all samples with MT	1564	2322	3886	1228	78.52	1764	75.97	2992	76.99	894	23.01
10	9	TiO_2 to P_2O_5 (M) all multinormal samples with MT	1118	1395	2513	846	75.7	1148	82.29	1994	79.35	519	20.65

different between the two groups. However, we were successful in using 9 major elements (excluding SiO_2) to discriminate these two settings. However, all 10 major element adjusted data were converted to isometric log-ratios following Egozcue et al. (2003) and used for the LDA and canonical analysis.

Because the LDA requires multivariate normality or multi-normality (Morrison, 1990), both the original concentrations as well as the ilr-transformed variables were separately evaluated for each tectonic group in the online computer program DOMuDAF (Verma et al., 2016) and multivariate discordant outlier-free, i.e., multinormal data were used for the LDA and canonical analysis. The multi-normality was also tested for the 9 major elements and the outlier-free data were used in the LDA and canonical analysis.

Similar procedure was developed for all 10 major and 6 trace elements (Cr, Nb, Ni, V, Y, and Zr). These trace elements were selected not only for their high discriminating power, but also because all of them, including all major elements, can be easily determined by one of the most common techniques of X-ray fluorescence spectrometry. This is not the case of other trace elements, such as the rare-earth elements, although they have also been proved to have high multidimensional discriminating power (e.g., Agrawal et al., 2008). Nevertheless, the selected trace elements will facilitate the application of the proposed procedure by most users. First, all 16 elements were readjusted to sum up to 100%, taking due care of correctly handling the measurement units as % m/m. Then, both the original concentrations and the ilr-transformed data were used for the LDA and canonical analysis.

Now, because the number of samples in our database with complete major and trace element data was much less (3886) than the total number in the complete database (7386), we also evaluated both M and MT data separately from only those samples having complete major and trace elements, i.e., 3886 samples. This allowed us to objectively evaluate the effect of increasing the dimensions in the solution as well as to compare the effect of the number of samples for the same dimensions.

Finally, the proposed method for application to samples from an unknown or complex tectonic setting has only two final solutions: (1) multi-normally distributed 9 ilr-transformed major elements (ilr_M) of the complete database (2788 for MOR and 2862 for OP; total of 5650 samples); and (2) multi-normally distributed 15 ilr-transformed major and trace elements (ilr_{MT}) of the database having complete data (1126 for MOR and 1732 for OP; total of 2858 samples).

We also note that it is not necessary to plot the samples in diagrams. The computer program presented here provides both the simple sample counting and the complex probability-based counting for a set of samples. Nevertheless, in this work we have included diagrams as a visual aid to the discrimination problem, because most people still prefer to see them. The probability-based solution is only briefly mentioned but can be consulted in the Excel files at http://tlaloc.ier.unam.mx after proper registration and log-in.

3. Results

We present and compare 10 different models for achieving discrimination of the MOR and OP tectonic settings. All results are summarized in Table 1.

3.1. Original 100% adjusted major element concentrations without transformation (two models of type M; item Nos. 1 and 2 in Table 1)

The 9 major element concentrations from TiO_2 to P_2O_5 (without SiO_2) in the complete dataset were successfully used to achieve percent success values (Table 1) of about 81.8% (3052 samples correctly discriminated out of 3730) for the MOR and 69.2% (2531 correctly classified out of 3656) for the OP, with total weighted average of about 75.6% (5583 out of 7386). The incorrect discrimination was about 24.4% (1803 out of 7386). Note that, from the concentrations of 9 elements in the complete dataset, the percent success values were drastically different for the MOR and OP settings (81.8% versus 69.2%), although the number of samples in both settings were approximately similar.

As required by the LDA and canonical analysis, the assumption of multi-normality for the MOR and OP groups, was tested online from DOMuDAF (Verma et al., 2016) in the 9 dimensions of major elements. The resulting censored data were used for the LDA and canonical analysis. The percent success (Table 1) slightly decreased to about 79.2% (2027 correctly classified out of 2558) for the MOR, but increased significantly to 82.9% (1524 out of 1839) for the OP. Thus, these two settings were discriminated with rather similar percent success (79.2% and 82.9%), probably as a result of multi-normality. The overall correct classification from the censored data increased to about 80.8% (increase of about 5.2% with respect to the use of all data) and correspondingly, the incorrect classification reduced to about 19.2% (decrease of 5.2% as compared to the use of all data).

3.2. Isometric log-ratio transformed major elements (two models of type ilr_M; item Nos. 3 and 4 in Table 1)

The 9 ilr variables from 10 major elements were used for the discrimination of the MOR and OP settings. The complete data set provided the success values of 74.2% (2767 out of 3730) for the MOR and

75.3% (2754 out of 3656) for the OP, with the overall correct discrimination of about 74.7%. The log-ratio transformation also yielded similar success (74.2% and 75.3%) for both groups. The incorrect discrimination was about 25.3%, slightly more than that for the original major elements, although the comparison should be done for the discrimination from multi-normally distributed data.

After the fulfilment of the multi-normality assumption in the ilr space, the percent success values were about 80.9% (2255 out of 2788) for the MOR and 81.1% (2321 out of 2862) for the OP, with the overall success of 81.0% and the incorrect classification of 19.0%. The fulfilment of the multi-normality assumption in the censored data not only rendered even more similar success (80.9% and 81.1%) for both groups but also increased the correct discrimination (and decreased the incorrect discrimination) by 6.3% as compared to the complete dataset. Therefore, we should not carry out the LDA and canonical analysis to the complete dataset, which does not comply with the assumption of multi-normality.

However, although the ilr transformation only marginally increased the success by about 0.2% as compared to the use of original concentrations, we will still use this transformation for routine applications, because it overcomes the closure and constant sum problem of compositional data and is likely to be robust against post-emplacement changes.

3.3. Original 100% adjusted major (M) and trace (T) elements without transformation (two models of type MT; item Nos. 5 and 6 in Table 1)

As for the M, all MT elements could not be used. The use of MT concentrations (14 elements, excluding SiO_2 and MnO) in all samples provided the success values of 90.0% (1408 out of 1564) and 79.8% (1852 out of 2322) for the MOR and OP, respectively. The percent success for both groups (90.0% and 79.8%) were significantly different. The overall success was about 83.9%, with incorrect discrimination of 16.1%.

The censored data increased the success to 94.5% (621 out of 657) and 90.2% (871 out of 966) for the MOR and OP, respectively, with the overall success of 91.9% and incorrect classification of only 8.1%. The two groups were discriminated by high and more similar success values (94.5% and 90.2%). Therefore, again when the multi-normality assumption was met, the success increased by about 8% (91.9% vs. 83.9%). However, the total number of samples representing the two settings significantly decreased from 3886 to only 1623.

3.4. Isometric log-ratio transformed major (M) and trace (T) elements (two models of type ilr_{MT}; item Nos. 7 and 8 in Table 1)

The ilr-transformed MT data showed the success of 80.9% (1266 out of 1564) and 86.8% (2015 out of 2321) for the MOR and OP, respectively, with the overall success of about 84.5% and the incorrect discrimination of about 15.5% (only slightly less than 16.1% from chemical concentrations). The censored data increased the respective success values to 88.5% (996 out of 1126) and 90.1% (1561 out of 1732). Both log-ratio transformation and multi-normality made the percent success values similar for both groups. The overall success also increased to about 89.5% (about 5% more than for the original ilr data), which was, however, 2.4% less than the 91.9% obtained for the element concentrations. Nevertheless, because the total number of samples (2858) for the ilr transformation were much higher than those for the original concentrations (1623), the former is more representative than the latter. It is, therefore, recommendable to use the log-ratio transformed data for discrimination.

3.5. Original 100% adjusted major (two models of type M) without transformation, same samples as the two models of type MT (item Nos. 9 and 10 in Table 1)

If we use the same samples for major elements that have complete data for MT, it will be easier to evaluate the effect of dimensionality in the solution of tectonic setting discrimination. Our database presented 3886 samples (1564 from the MOR and 2322 from the OP), whose major element concentrations provided the success of about 78.5% and 76.0%, with the overall average success of about 77.0% and the incorrect discrimination of 23.0%.

The complete database (7386 samples; 3730 and 3656 for the MOR and OP, respectively), for comparison, had given average weighted success of 75.6% (item No. 1 in Table 1), slightly lower (1.4%) than the success from the 3886 samples with complete MT data. Therefore, increasing the number of samples in the database will not always increase the success values. In this case, the success values seem to approximately stabilise around 76%, provided the representatively is achieved by the sampling in the field.

We then used the multi-normally distributed major element data having complete MT data and obtained the success values of about 75.7% (846 out of 1118) for the MOR and 82.3% (1148 out of 1395) for the OP, with overall success of 79.3% and incorrect discrimination of 20.7%. The use of higher number of samples (3551; item No. 2 in Table 1) had given a slightly higher success values of about 80.8% (about 1.5% higher than 79.3% for item No. 10; Table 1). Again, the success values seem to stabilise around 80%.

4. Selection of multidimensional discrimination for future applications

Because the possibilities for multidimensional discrimination are too many (a total of 10; Table 1), we should decide on the method that should be routinely applied to decipher the unknown setting indicated by a set of test or application samples. From the criteria of correct discrimination, multi-normality assumption, and representativeness of the two tectonic settings, we decided to use the multi-normally distributed ilr-transformed major elements (called ilr_M model) and combined major and trace elements (ilr_{MT} model) for routine use (item nos. 4 and 8, respectively, in Table 1).

The respective discriminant equations for ilr_M and ilr_{MT} were as follows (coefficients rounded to 5 decimal places although unrounded values were programmed in MOROPdisc described in Section 5):

$$\begin{aligned} DF_{(MOR-OP)M} = {} & (4.58733 \times ilr1_{TiM}) + (6.38983 \times ilr2_{AlM}) + (5.25387 \times ilr3_{FeTM}) \\ & + (-1.51693 \times ilr4_{MnM}) + (-0.30061 \times ilr5_{MgM}) \\ & + (-3.87204 \times ilr6_{CaM}) + (-4.33842 \times ilr7_{NaM}) \\ & + (0.91691 \times ilr8_{KM}) + (-1.04554 \times ilr9_{PMT}) \\ & + (-1.67031) \end{aligned} \quad (1)$$

$$\begin{aligned} DF_{(MOR-OP)MT} = {} & (0.55309 \times ilr1_{TiMT}) + (0.46880 \times ilr2_{AlMT}) \\ & + (1.67225 \times ilr3_{FeTMT}) + (-1.46860 \times ilr4_{MnMT}) \\ & + (-1.97055 \times ilr5_{MgMT}) + (-4.20578 \times ilr6_{CaMT}) \\ & + (-2.37209 \times ilr7_{NaMT}) + (-0.22495 \times ilr8_{KMT}) \\ & + (-1.16912 \times ilr9_{PMT}) + (-0.60424 \times ilr10_{CrMT}) \\ & + (0.13069 \times ilr11_{NbMT}) + (0.02033 \times ilr12_{NiMT}) \\ & + (0.31134 \times ilr13_{VMT}) + (-4.82283 \times ilr14_{YMT}) \\ & + (-0.07804 \times ilr15_{ZrMT}) + (31.76267) \end{aligned} \quad (2)$$

The discrimination based on M, i.e., ilr_M model, is to be used only when the complete data for MT, i.e., ilr_{MT} model, are not available. The training set samples from both settings were plotted in diagrams corresponding to the ilr_M (Fig. 2A) and ilr_{MT} (Fig. 2B) models.

The correct discrimination, centroid and boundary locations are shown in both figures (Fig. 2A, B). The overlap (incorrect discrimination) was around 19% for ilr_M (Fig. 2A; Table 1), i.e., a total of about 19% of the MOR and OP samples plotted incorrectly towards the left and right of the boundary ($B_{(MOR-OP)M}$), respectively. The distance of the two centroids in the DF space was about 1.67958 (Fig. 2A).

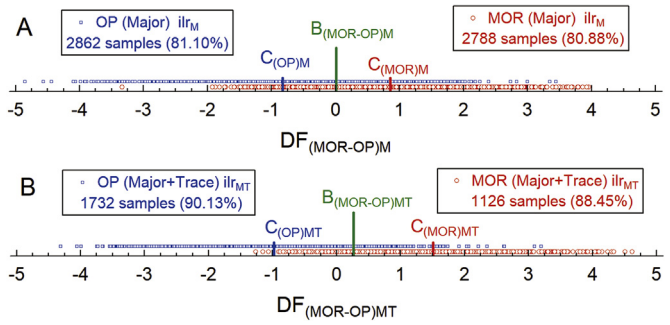

Fig. 2. One-axis ($DF_{(MOR-OP)M}$ and $DF_{(MOR-OP)MT}$) multidimensional diagrams for the discrimination of mid-ocean ridge (MOR) and oceanic plateau (OP) settings showing the training set samples; more details are given as insets. (A) Isometric log-ratio (ilr) transformed major element (M) based, ilr_M model (MOR centroid $C_{(MOR)M} = 0.85079$ and OP centroid $C_{(OP)M} = -0.82879$; tectonic field boundary $B_{(MOR-OP)M} = 0.01100$). (B) Isometric log-ratio (ilr) transformed major and trace element (MT) based, ilr_{MT} model (MOR centroid $C_{(MOR)M} = 1.50667$ and OP centroid $C_{(OP)M} = -0.97951$; tectonic field boundary $B_{(MOR-OP)M} = 0.26358$).

For the ilr_{MT} (Fig. 2B), the incorrect discrimination was only about 10.5% (Table 1). The correct discrimination is correspondingly much higher than the ilr_M model (Fig. 2B). The two centroids are far away from one another (2.48618), more than the ilr_M model (1.67958). The farther the two centroids in a diagram are, the higher success values are expected (Verma, 2020). Therefore, the ilr_{MT} model is likely to give higher success than the ilr_M model (Fig. 2B vs. Fig. 2A) for future applications and is, therefore, recommended when complete major and trace element data are available.

5. Computer program

To facilitate the use of our diagrams (major elements M through isometric log-ratio transformation model ilr_M and combined major and trace elements MT through model ilr_{MT}; Figs. S1–S3), we have written an online computer program MOROPdisc in Java and ZK Framework, which is available at our web portal http://tlaloc.ier.unam.mx for use by anyone after registration and log-in.

Basically, the Validation module (Fig. S1) of the MOROPdisc software evaluates the input file for possible typographical or other errors and sends an error message, if any, to request the user to correct them in the original Excel program. To easily achieve an error-free file, it is recommended to download the appropriate template from http://tlaloc.ier.unam.mx and modify it accordingly in the original Excel® program for use at this portal, taking due care of first fully eliminating all existing data rows, except the headers before entering new data. In other words, no empty cells should be present after eliminating any data therein (Java has conflicts with such cells and might mark an error in that empty cell).

Once the input file is error-free, the user can open this file in the online program. More information is given in Figs. S2 and S3. The user can opt for processing the data for discriminating the tectonic setting of samples (MOR or OP) or evaluating the robustness (uncertainty propagation or post-emplacement changes). The correct format of the input file, however, is a must for a successful use of the program.

Only the major element (M) option or both major and combined major and trace elements (M and MT) followed by ilr-transformation, i.e., the ilr_M and ilr_{MT} models, can be called for discriminating the tectonic settings. For the robustness option, new compositions are simulated from the Monte Carlo method (2200 for the uncertainty propagation or generally a lesser number for the post-emplacement option as required by the individual applications). The post-emplacement option stops when the tectonic setting of the sample changes or any of the following conditions is violated: (i) $99\% > (SiO_2)_{adj} > 31\%$; (ii) any adjusted major (oxide) concentration >0.002%; and (iii) any adjusted trace element concentration in % m/m > 0.00001%. These conditions could be considered somewhat arbitrary (e.g., the highest value of $(SiO_2)_{adj}$ could be 98% m/m or less instead of 99% m/m or the trace element condition could be 0.00002% for some elements instead of 0.00001% currently set for all elements), but were imposed to keep the post-emplacement changed adjusted compositions reasonably consistent with an igneous rock. In the post-emplacement module, depending upon the chosen step sizes, the altered rock composition may evolve to unreasonable values for it to be an igneous rock. Therefore, we may have to learn more about imposing additional conditions to keep the evolved rock compositions as an igneous rock.

For all options, the program adjusts the data, as either M or MT, to 100% on an anhydrous basis with total Fe as $Fe_2O_3^t$. Then, it calculates the ilr-transformations (ilr_M and ilr_{MT}) and the discriminant functions ($DF_{(MOR-OP)M}$ and $DF_{(MOR-OP)MT}$ from unrounded coefficients in Eqs. (1) and (2)). Adequate reports are generated for each option, which are called as follows: (i) the "Report_Result" file containing information for the individual samples; and (ii) the "Report_Summary" file having the statistical information for the set of samples. Both simple counting of samples as well as probability-based decisions are then printed out for the user to know the outcome of the samples in terms of these two tectonic settings.

MOROPdisc also enables the user to test the robustness of this multidimensional discrimination against uncertainty propagation and post-emplacement compositional changes (Fig. S3). The output file generated by MOROPdisc in the "Downloads" folder of the user's computer does not have the input file name. However, the user can change its name and move it to a suitable file folder, e.g., to the original input file folder.

The "Report_Result" file provides the necessary discriminant function values for all samples of a set under study, which can be used for plotting the samples in diagrams if desired by the user.

6. Test case studies

Our test studies are for samples not included in the database for proposing the multidimensional discrimination, because this would be an objective procedure. Arbitrarily, for these tests, we decided to present only those cases that reported at least 5 samples, preferably with both major and trace elements.

6.1. First test study (expected setting of MOR)

The geochemical data for 10 samples of altered lower crustal gabbroic rocks from the Atlantis Bank, Southwest Indian Ridge, were compiled from Hertogen et al. (2002). These 10 samples had complete data for the major elements, but only 4 samples were complete in the combined major and trace elements. Therefore, we present results of only the ilr_M discrimination (Fig. 3). The data (see the input Excel file at the web portal http://tlaloc.ier.unam.mx) were processed in MOROPdisc. The DF_{ilrM} values from the MOROPdisc program (the Result file) showed that all 10 samples plotted well within the MOR field (Fig. 3). The mean probability value of these samples ($n = 10$) for the MOR field was very high (0.9636 ± 0.0499; the ±value is the standard deviation; the corresponding

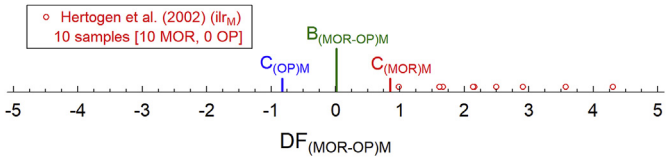

Fig. 3. One-axis $DF_{(MOR-OP)M}$ multidimensional diagram for the discrimination of mid-ocean ridge (MOR) and oceanic plateau (OP) settings showing the gabbroic rock samples of the Atlantis Bank, SW Indian Ridge (Hertogen et al., 2002); centroids and boundary values are given in Fig. 2 and more details are in insets.

probability for the OP setting was very low, 0.0364), clearly suggesting the MOR setting for these altered samples, in agreement with their location at the Southwest Indian Ridge.

MOROPdisc also provided the probability-based sample counts (96.4% total probability for the MOR and only 3.6% for the OP; see the output summary excel file at http://tlaloc.ier.unam.mx). For the total of 10 samples, the probability count will amount to 10 samples (in fact, 9.64 samples to be exact in terms of probability, which when rounded to an integer number of samples will be 10) plotting in the MOR field and none (0.36 samples in terms of probability, which when rounded to an integer will be 0) in the OP field. This confirmed the decision of a MOR setting for the studied samples from the Atlantis Bank from both sample and probability-based counting.

In this particular case, it would make no difference whether to base the decision on sample counts (all 10 samples plotted in the MOR field; Fig. 3) or to use the decision on probability values (see the full Result and Summary files at http://tlaloc.ier.unam.mx). However, the probability-based counting may be more useful for undecisive cases as the ilr_M results in Section 6.4. We, therefore, provide details on the probability-based decision only when the sample counting was indecisive.

Henceforth, we will refer to the "Report_Result" and "Report_Summary" excel files, without citing them; they can be readily consulted at http://tlaloc.ier.unam.mx after proper registering and logging in on to this portal (in case of difficulty, please contact the servicing manager aqr@ier.unam.mx or the first author of this paper spv@ier.unam.mx).

6.2. Second test study (expected setting of MOR)

Nakamura et al. (2007) presented geochemical data for 128 hydrothermally altered rock samples from the SW Indian Ridge close to the Rodriguez triple junction, of which 86 samples had complete data for the combined major and trace elements. The DF values for the ilr_M and ilr_{MT} models are plotted in Fig. 4A and B, respectively. Both diagrams (Fig. 4A, in which 121 out of 128 samples plotted in the MOR field and Fig. 4B, 78 out of 86) and the high probability values for the MOR setting ($n = 121$, 0.938 ± 0.067 and $n = 83$, 0.965 ± 0.081, respectively, for the ilr_M and ilr_{MT}) clearly indicated the expected MOR setting. The probability-based counting confirmed this inference.

6.3. Third test study (expected setting of OP)

Kerr et al. (2002) reported geochemical data on 19 samples of basaltic, komatiitic, and picritic rocks from the accreted portion of the 90 Ma Colombian–Caribbean Oceanic Plateau. We processed these samples in MOROPdisc program. The ilr_M and ilr_{MT} models showed, respectively, that 16 out of 19 samples (Fig. 5A) and 18 out of 19 samples (Fig. 5B) plotted in the OP field. The mean probability for the 16 samples correctly

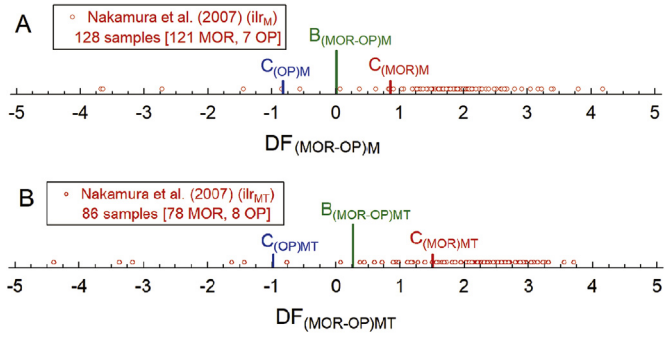

Fig. 4. One-axis multidimensional diagrams (A) $DF_{(MOR-OP)M}$ and (B) $DF_{(MOR-OP)MT}$ for the discrimination of mid-ocean ridge (MOR) and oceanic plateau (OP) settings showing the hydrothermally altered rock samples from the SW Indian Ridge reported by Nakamura et al. (2007); centroids and boundary values are given in Fig. 2 and more details are in insets.

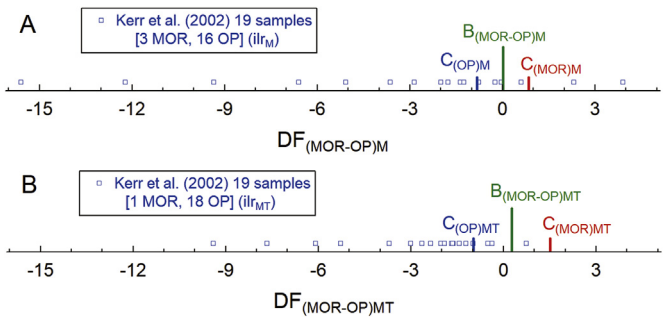

Fig. 5. One-axis multidimensional diagrams (A) $DF_{(MOR-OP)M}$ and (B) $DF_{(MOR-OP)MT}$ for the discrimination of mid-ocean ridge (MOR) and oceanic plateau (OP) settings showing the igneous rock samples from the accreted portion of the 90 Ma Colombian–Caribbean oceanic plateau reported by Kerr et al. (2002); centroids and boundary values are given in Fig. 2 and more details are in insets.

classified as OP was 0.905 ($\pm$0.147) from the ilr_M model and that for the 18 samples from the ilr_{MT} model was still somewhat higher (0.977 ± 0.047). The probability-based result summary from both models also indicated the expected setting of OP for the accreted portion of the Colombian–Caribbean oceanic plateau.

6.4. Fourth test study (expected setting of OP)

We compiled the geochemical data for 26 samples of massive and pillow lavas from the Azuero Marginal Complex (Azuero Plateau of Coniacian–early Santonian, ~89–85 Ma) reported by Buchs et al. (2010), 23 of which had complete major and trace element data. The sample counting from the ilr_M model did not provide any decision because the same number of samples (13 each) plotted in the MOR and OP fields (Fig. 6A). However, the ilr_{MT} model clearly indicated the OP setting because all 23 samples plotted in the OP field (Fig. 6B).

The probability-based counting was able to solve the indecision of the ilr_M model, because equivalent to 12 and 14 samples, respectively, corresponded to the MOR and OP settings. The decision was in favour of the OP setting, although with a marginal success of only 54%. For the ilr_{MT} model, the probability-based decision of the OP setting was, however, confirmed with a relatively high success of about 80%.

In order to better understand the performance of multidimensional discrimination diagrams and varying results of the ilr_M and ilr_{MT} models, we need to have access to individual error or total uncertainty on each geochemical datum, which will only be possible if the researchers start reporting total uncertainties (combined calibration and individual run uncertainties of the "unknown" samples, and not simply the repeat run errors) as recently illustrated by Verma et al. (2018, 2019) in their preferred uncertainty-weighted least-squares linear regression model for the calibration of X-ray fluorescence spectrometry and by Torres-Sánchez et al. (2019) who presented data tables with total uncertainty of individual major elements in each rock sample.

We should then be able to evaluate each sample in the Robustness module of MOROPdisc and thus learn more on the robustness of individual sample compositions. Nevertheless, we may point out that the indecision is more likely to occur with the major element discrimination (ilr_M) instead of the combination of major and trace elements (ilr_{MT}), because, during the training, the former proposal (Fig. 2B) was obtained with lesser percent success (81.0% vs. 89.5%; Table 1) than the latter (Fig. 2B).

7. Application studies

We present two application studies each of the ophiolite tectonic setting and of Precambrian rocks. We note that the existing multidimensional diagrams (e.g., Verma et al., 2006; Agrawal et al., 2008;

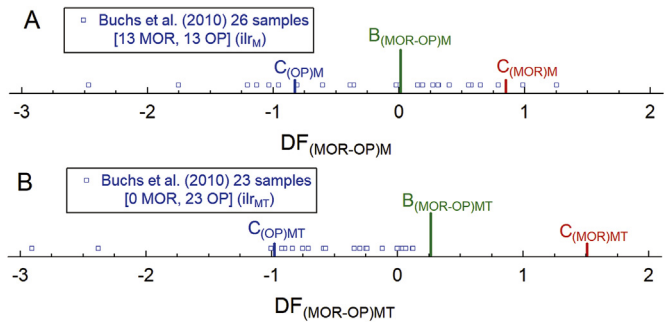

Fig. 6. One-axis multidimensional diagrams (A) $DF_{(MOR-OP)M}$ and (B) $DF_{(MOR-OP)MT}$ for the discrimination of mid-ocean ridge (MOR) and oceanic plateau (OP) settings showing the massive and pillow lava samples from the Azuero Marginal Complex reported by Buchs et al. (2010); centroids and boundary values are given in Fig. 2 and more details are in insets.

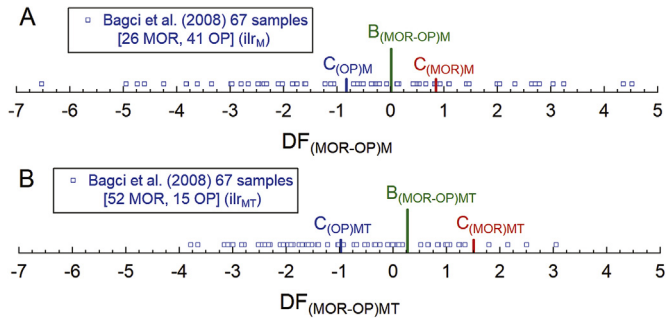

Fig. 8. One-axis multidimensional diagrams (A) $DF_{(MOR-OP)M}$ and (B) $DF_{(MOR-OP)MT}$ for the discrimination of mid-ocean ridge (MOR) and oceanic plateau (OP) settings showing the igneous rock samples from the Kizildag (Hatay) ophiolite, Southern Turkey (Bagci et al., 2008); centroids and boundary values are given in Fig. 2 and more details are in insets.

Verma and Agrawal, 2011) should always be used before the application of MOROPdisc.

For the ophiolites, subduction setting is an important option, which can be deduced from the already available multidimensional diagrams (Verma et al., 2006; Agrawal et al., 2008; Verma and Agrawal, 2011). This procedure was adopted by Verma et al. (2015), who used their preliminary discrimination scheme to achieve MOR-OP discrimination. However, without the MOR-OP discrimination (Verma et al., 2015; this work), the OP setting cannot be inferred for any of the ophiolitic complex. Therefore, we decided to apply the present discrimination scheme to understand if an ophiolitic complex has more affinity with the MOR than with the OP or vice versa.

7.1. First application study: Mineoka ophiolite

Geochemical data for 21 igneous rock samples from the Tertiary Mineoka ophiolite, southern Boso Peninsula, Japan (Hirano et al., 2003), were used to infer their greater affinity with either MOR or OP. Both ilr_M and ilr_{MT} models indicated the MOR affinity because, respectively, 16 (Fig. 7A) and 17 (Fig. 7B) samples out of 21 plotted in this field. The probability-based counting fully confirmed this inference.

7.2. Second application study: Hatay ophiolite

Major and trace element data for 67 samples of igneous rocks from the Kizildag (Hatay) ophiolite, Southern Turkey, were compiled from Bagci et al. (2008). These authors stated that the Hatay ophiolite is one of the best-preserved oceanic lithospheric remnants in southern Turkey. Our aim was to test the greater affinity of this ophiolite with either the MOR or the OP. The ilr_M model showed that 41 out of 67 samples plotted in the OP field (Fig. 8A), whereas the ilr_{MT} model indicated still higher number (52 out of 67) of samples in the OP field (Fig. 8B). The probability-based counting confirmed the affinity with the OP setting.

7.3. Third application study: Precambrian birimian terranes of West Africa

Twenty-five igneous rock samples from 2.1 Ga Birimian terranes of West Africa (Mauritania, Senegal, Ivory Coast, Burkina Faso, and Niger) were compiled from Abouchami et al. (1990) and processed in MOROPdisc. In the major element-based diagram (ilr_M model), 18 samples (out of 25) plotted in the OP field (Fig. 9A). Only 5 samples had complete major and trace element data, all of which plotted in the OP field (ilr_{MT} model; Fig. 9B). Incidentally, these 5 samples were also discriminated as OP from the ilr_M model. Therefore, the OP setting was indicated for these Precambrian rocks from West Africa (Fig. 9A and B). We also note that if the MT data for a greater number of samples were available from these wide areas (Fig. 1), it would be advisable to evaluate them as different groups, each from a limited geographical area.

7.4. Fourth application study: Precambrian amphibolite-gneiss

For the final (fourth) application, we compiled complete major and trace element data for 23 metamorphic rock samples of 2236 ± 55 Ma-old Algodões amphibolite–tonalite gneiss sequence, Borborema Province, NE Brazil, from Martins et al. (2009) and processed them in MOROPdisc. The ilr_M model showed that 13 out of 23 samples plotted in the OP field (Fig. 10A), whereas the ilr_{MT} model gave much higher success with 22 out of 23 samples plotting in the OP field (Fig. 10B). Therefore, from both diagrams (Fig. 10A and B), the OP setting was

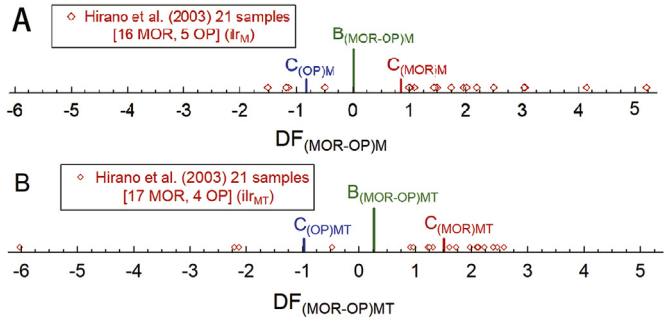

Fig. 7. One-axis multidimensional diagrams (A) $DF_{(MOR-OP)M}$ and (B) $DF_{(MOR-OP)MT}$ for the discrimination of mid-ocean ridge (MOR) and oceanic plateau (OP) settings showing the samples of the Tertiary Mineoka ophiolite, southern Boso Peninsula, Japan reported by Hirano et al. (2003); centroids and boundary values are given in Fig. 2 and more details are in insets.

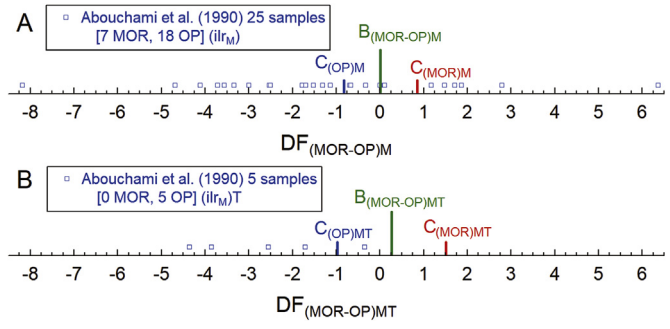

Fig. 9. One-axis multidimensional diagrams (A) $DF_{(MOR-OP)M}$ and (B) $DF_{(MOR-OP)MT}$ for the discrimination of mid-ocean ridge (MOR) and oceanic plateau (OP) settings showing the 2.1 Ga igneous rock samples from the Birimian terranes of West Africa (Abouchami et al., 1990); centroids and boundary values are given in Fig. 2 and more details are in insets.

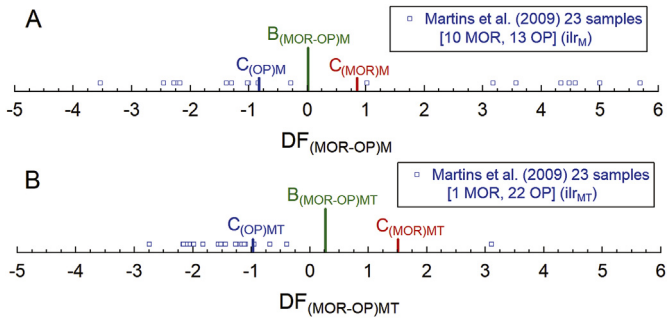

Fig. 10. One-axis multidimensional diagrams (A) $DF_{(MOR-OP)M}$ and (B) $DF_{(MOR-OP)MT}$ for the discrimination of mid-ocean ridge (MOR) and oceanic plateau (OP) settings showing the 2.236 Ga Algodões amphibolite–tonalite gneiss sequence, Borborema Province, NE Brazil (Martins et al., 2009); centroids and boundary values are given in Fig. 2 and more details are in insets.

confirmed for these Precambrian metamorphosed rocks.

8. Robustness module of MOROPdisc

The robustness module allows us to evaluate the effects of analytical errors or uncertainties as well as post-emplacement alteration changes in the field and in the laboratory. We briefly comment on the robustness against these processes from four specific examples (Table 2). As we have shown in these examples, the user can evaluate any sample or process from this module of MOROPdisc. For this, an input file (distinct files for the uncertainty propagation and post-emplacement changes) should be prepared and processed accordingly in MOROPdisc. The results of both processes (analytical uncertainties and post-emplacement gain or loss of elements) are presented in Tables 3 and 4, respectively, for uncertainty propagation and post-emplacement changes. Similarly, we also evaluated the robustness of single element changes (gain or loss; one element at a time) and documented the results in Tables 5 and 6, respectively, for the ilr_M and ilr_{MT} models, respectively.

Importantly, the robustness module enables the user to test his or her own samples for stability against both uncertainty propagation and post-emplacement changes.

8.1. Uncertainty propagation

For uncertainty propagation, we used the examples of the centroids of the MOR (1126 samples) and OP (1732 samples) as representative of the respective chemical compositions (Item No. 8 in Table 1). Because the total analytical uncertainties are not generally available for individual data as recently pointed out (Verma et al., 2018, 2019; Torres-Sánchez et al., 2019; Verma, 2020), we calculated, for illustration purposes, the 99% uncertainty values for the samples of the database used for the ilr_{MT} model and assigned them to each respective centroid concentration values. These two Excel files (data summarized in Table 2) were processed in the Robustness module of MOPOPdisc (Fig. S3).

The resulting simulated data (2200 replicates for each example) are plotted in Fig. 11A for ilr_M and Fig. 11B for the ilr_{MT} model, along with the centroid of the respective chemical compositions. Note that the centroids of the chemical compositions do not coincide with those of the discriminant functions (Fig. 11A and B), because the nonlinear ilr functions are involved in the process. All replicates plotted in the field of the respective tectonic setting, far away from the tectonic field boundaries (Fig. 11A and B), confirming thus the robustness of the multidimensional solution against analytical uncertainties. However, a greater stability or robustness of the ilr_{MT} model as compared to the ilr_M model is also clear, because the replicates plot closer to the dividing boundary in Fig. 11A (ilr_M model) than Fig. 11B (ilr_{MT} model). Therefore, with somewhat larger uncertainties, there will be mis-discrimination in Fig. 11A as compared to Fig. 11B.

Similar examples can be used to learn the maximum uncertainty values that may still give an acceptable solution (i.e., maintain the same tectonic setting of the initial composition) to any given sample. To provide guidelines about data quality required for a satisfactory solution of the tectonic setting is an important aspect of MOROPdisc.

8.2. Post-emplacement changes

8.2.1. Gain or loss of multiple elements

Numerous studies have been carried out on post-emplacement changes caused by both low and high temperature alteration (e.g., Humphris and Thompson, 1978; Mottl and Holland, 1978; Seyfried et al., 1978; Staudigel and Hart, 1983; Alt et al., 1986; Jochum and Verma, 1996; Torres-Alvarado et al., 2007; Pandarinath et al., 2008; Smith-Duque, 2009; Marks et al., 2010; Alacali and Savascin, 2015; Patten et al., 2016). The low temperature seawater, hydrothermal or metasomatic alteration and weathering on land could be quite complex with conflicting results and may require an adequate computer program to evaluate them in multidimensions. The post-emplacement changes caused by weathering, such as Fe oxidation, will not affect the discrimination, because total Fe concentration expressed as one oxidation state will not change significantly during Fe oxidation.

The basic idea was to illustrate the robustness of the multidimensional system from two examples, one each for the MOR and OP centroid sample compositions subjected to seawater alteration. The readers can easily test other examples by preparing the excel input file and running it in MOROPdisc.

For testing compositional changes, we prepared excel templates with the relative changes (gain or loss in % mass/mass unit) reported by different authors so that several steps could be tested until any of the

Table 2
Initial input information for robustness evaluation of uncertainty propagation and post-emplacement compositional changes.

Element (% m/m or μg/g)	Mid-Ocean Ridge (MOR)			Oceanic Plateau (OP)		
	Centroid $\bar{x}$	Uncertainty u_{99}	Step (% gain/loss)	Centroid $\bar{x}$	Uncertainty u_{99}	Step (% gain/loss)
SiO_2	49.895	0.057	0.6	48.820	0.112	0.6
TiO_2	1.4690	0.0282	−0.02	1.915	0.052	−0.02
Al_2O_3	14.779	0.074	0.02	14.606	0.083	0.02
$Fe_2O_3^t$	11.607	0.114	0.02	12.557	0.104	0.02
MnO	0.18660	0.00196	0.05	0.18675	0.00224	0.05
MgO	7.593	0.066	0.8	7.710	0.140	0.8
CaO	11.487	0.059	−0.3	10.844	0.088	−0.3
Na_2O	2.5530	0.0296	0.4	2.4981	0.0379	0.4
K_2O	0.1712	0.0124	−0.2	0.5350	0.0388	−0.2
P_2O_5	0.1802	0.0080	−0.02	0.2425	0.0128	−0.02
Cr	252.2	8.6	−0.2	248.9	14.6	−0.2
Nb	4.366	0.365	−0.2	15.70	1.15	−0.2
Ni	93.52	3.42	−0.5	116.2	5.9	−0.5
V	315.96	4.33	−1	317.59	4.55	−1
Y	33.39	0.61	0.5	27.49	0.48	0.5
Zr	92.94	2.43	0.5	128.8	5.1	0.5

Table 3
Output information for robustness evaluation of post-emplacement compositional changes in the major elements of the MOR and OP centroids.

Element	Initial composition (% m/m or μg/g) or mass units	Final mass in the field (mass units)	Final concentration in laboratory analysis (adj % m/m)	Maximum mass change in the field (gain or loss, % m/m)	Maximum mass change in laboratory (gain or loss, % m/m)
MOR centroid					
SiO_2	49.895	1711.842	65.50	3331	31.1
TiO_2	1.4690	1.305	0.050	−11.1	−96.6
Al_2O_3	14.779	16.633	0.64	12.5	−95.7
$Fe_2O_3^t$	11.607	13.063	0.50	12.5	−95.7
MnO	0.18660	0.251	0.0096	34.3	−94.8
MgO	7.593	842.535	32.2	10996	324.0
CaO	11.487	1.946	0.075	−83.1	−99.4
Na_2O	2.5530	27.019	1.036	958.3	−59.6
K_2O	0.1712	0.052	0.0020	−69.4	−98.8
P_2O_5	0.1802	0.160	0.0062	−11.1	−96.6
OP centroid					
SiO_2	48.82	60.19	53.172	23.3	8.8
TiO_2	1.915	1.902	1.680	−0.70	−12.4
Al_2O_3	14.606	14.709	12.993	0.70	−11.1
$Fe_2O_3^t$	12.557	12.645	11.171	0.70	−11.1
MnO	0.18675	0.19	0.168	1.76	−10.2
MgO	7.71	10.19	9.002	32.2	16.7
CaO	10.844	9.762	8.623	−10.0	−20.5
Na_2O	2.4981	2.873	2.538	15.0	1.50
K_2O	0.535	0.499	0.441	−6.8	−17.7
P_2O_5	0.2425	0.241	0.213	−0.70	−12.4

conditions was unsatisfied or the tectonic setting changed (see Section 5 for conditions). For those elements, for which no specific or unambiguous information on alteration was available, we arbitrarily assigned small changes to show that the computer program can deal with changes (gain or loss) in all elements.

The results for the MOR and OP compositions (see Table 2 for the steps) are plotted in Fig. 12A for the major elements (ilr_M) and Fig. 12B for the combined major and trace elements (ilr_{MT}). The respective output summaries are presented in Tables 3 and 4. We will explain in detail the major element evaluation of the MOR centroid (Fig. 12A; Table 3).

The post-emplacement changed compositions of the MOR centroid after each step remained in the MOR setting for 591 steps (Fig. 12A). Let us assume that we have, in the field, a total of 100 mass units, e.g., 100 g, of the MOR centroid composition, the initial composition can represent the mass of individual elements (Table 3) in the total of 100 g. For example, SiO_2 mass initially was 49.895 g, similar mass values for all other major elements are listed in the second column (first data column) of Table 3. The 591 steps of post-emplacement gain increased the mass of

Table 4
Output information for robustness evaluation of post-emplacement compositional changes in the major and trace elements of the MOR and OP centroids.

Element	Initial composition (% m/m or μg/g) or mass units	Final mass in the field (mass units)	Final concentration in laboratory analysis (adj % m/m)	Maximum mass change in the field (gain or loss, % m/m)	Maximum mass change in laboratory (gain or loss, % m/m)
MOR centroid					
SiO_2	49.895	1060.780	68.02	2026	36.3
TiO_2	1.4690	1.326	0.0850	−9.7	−94.2
Al_2O_3	14.779	16.369	1.050	10.8	−92.9
$Fe_2O_3^t$	11.607	12.856	0.824	10.8	−92.9
MnO	0.18660	0.241	0.0154	29.1	−91.7
MgO	7.593	445.395	28.56	5766	276.1
CaO	11.487	2.474	0.159	−78.5	−98.6
Na_2O	2.5530	19.633	1.259	669	−50.7
K_2O	0.1712	0.062	0.00395	−64.0	−97.7
P_2O_5	0.1802	0.163	0.0104	−9.7	−94.2
Cr	252.2	90.668	0.000581	−64.0	−97.7
Nb	4.366	1.570	0.0000101	−64.0	−97.7
Ni	93.52	7.219	0.0000463	−92.3	−99.5
V	315.96	1.859	0.0000119	−99.4	−100.0
Y	33.39	427.045	0.00274	1179	−17.9
Zr	92.94	1188.667	0.00762	1179	−17.9
OP centroid					
SiO_2	48.82	68.247	55.52	39.8	13.7
TiO_2	1.915	1.894	1.540	−1.11	−19.6
Al_2O_3	14.606	14.77	12.016	1.13	−17.7
$Fe_2O_3^t$	12.557	12.698	10.330	1.13	−17.7
MnO	0.18675	0.192	0.156	2.84	−16.3
MgO	7.71	12.046	9.799	56.2	27.1
CaO	10.844	9.165	7.455	−15.5	−31.2
Na_2O	2.4981	3.124	2.541	25.1	1.73
K_2O	0.535	0.478	0.389	−10.6	−27.3
P_2O_5	0.2425	0.24	0.195	−1.11	−19.6
Cr	248.9	222.503	0.0181	−10.6	−27.3
Nb	15.7	14.035	0.00114	−10.6	−27.3
Ni	116.2	87.76	0.00714	−24.5	−38.6
V	317.59	180.9	0.0147	−43.0	−53.7
Y	27.49	36.347	0.00296	32.2	7.6
Zr	128.8	170.30	0.0139	32.2	7.6

Table 5
Robustness of major element based diagram (ilr_M model) against post-emplacement changes of one element at a time for step size of ±0.1% in MOR and OP centroids.

Element	Gain					Loss				
	# steps	Field (%)	Laboratory (%)		Cause for change for the next step after the # steps	# steps	Field (%)	Laboratory (%)		Cause for change for the next step after the # steps
			Evaluated element	All other elements				Evaluated element	All other elements	
MOR centroid										
SiO_2	5141	+16,945	+99	−99	$(SiO_2)_{adj}$ too large; $(K_2O)_{adj}$ too small	105	−10	−5.3	+5.3	Tectonic setting changed
TiO_2	880	+141	+136	−2	Tectonic setting changed	6611	−99.9	−99.9	+1.49	$(TiO_2)_{adj}$ too small
Al_2O_3	115	+12	+10	−1.8	Tectonic setting changed	7359	−99.9	−99.9	+17	Tectonic setting changed
$Fe_2O_3^t$	99	+11	+9.2	−1.2	Tectonic setting changed	6338	−99.8	−99.8	+13	Tectonic setting changed
MnO	5880	+35,576	+21,335	−40	$(SiO_2)_{adj}$ too small	4536	−99	−99	+0.185	$(MnO)_{adj}$ too small
MgO	673	+96	+83	−6.8	Tectonic setting changed	8317	−10	−10	+8.2	$(MgO)_{adj}$ too small
CaO	1914	+577	+307	−40	$(SiO_2)_{adj}$ too small	202	−18	−17	+2.16	Tectonic setting changed
Na_2O	3297	+2599	+1522	−40	$(SiO_2)_{adj}$ too small	150	−14	−14	+0.36	Tectonic setting changed
K_2O	625	+87	+87	−0.1	Tectonic setting changed	4449	−99	−99	+0.17	$(K_2O)_{adj}$ too small
P_2O_5	5914	+36,809	+22,083	−40	$(SiO_2)_{adj}$ too small	613	−46	−46	+0.0828	Tectonic setting changed
OP centroid										
SiO_2	209	+23	+11	−10	Tectonic setting changed	801	−55	−39	+37	$(SiO_2)_{adj}$ too small
TiO_2	3522	+3279	+1975	−39	$(SiO_2)_{adj}$ too small	1749	−83	−82	+1.61	Tectonic setting changed
Al_2O_3	1668	+430	+225	−39	$(SiO_2)_{adj}$ too small	229	−21	−18	+3.1	Tectonic setting changed
$Fe_2O_3^t$	1793	+500	+269	−39	$(SiO_2)_{adj}$ too small	197	−18	−16	+2.31	Tectonic setting changed
MnO	5824	+33,634	+20,613	−39	$(SiO_2)_{adj}$ too small	4537	−99	−99	+0.185	$(SiO_2)_{adj}$ too small
MgO	2214	+814	+461	−39	$(SiO_2)_{adj}$ too small	1337	−74	−72	+6	$(SiO_2)_{adj}$ too small
CaO	403	+50	+42	−5.1	Tectonic setting changed	8709	−10	−10	+12	$(SiO_2)_{adj}$ too small
Na_2O	298	+35	+34	−1	Tectonic setting changed	7152	−99.9	−99.9	+2.56	$(Na_2O)_{adj}$ too small
K_2O	4776	+11,735	+7168	−39	$(SiO_2)_{adj}$ too small	1241	−71	−71	+0.382	Tectonic setting changed
P_2O_5	1221	+239	+237	−1	Tectonic setting changed	4798	−99	−99	+0.241	$(P_2O_5)_{adj}$ too small

SiO_2 to about 1701.6 g in the field. Other final mass values of the post-emplacement changed sample in the field are listed in the third column (i.e., second data column) of Table 3; the new mass of all elements summed up to 2597.803 g.

When this altered sample is brought to the laboratory and its major element contents are determined, the final mass in the field would correspond to the concentration values listed in the third data column in Table 3. For example, the final mass of 1711.8 g SiO_2 would correspond to 65.50% m/m (1711.8 g SiO_2 out of the total mass of 2614.8 g).

We can also interpret these simulated data in terms of the percent gain or loss of each element, both in the field and in the laboratory. For example, the final sample (after 591 steps of changes) would have gained +3331% SiO_2 in the field (fourth data column in Table 3), which would imply the gain of +31.1% only in the laboratory analysis of this final sample (the final column in Table 3).

Although we assumed in Table 2 that six elements had positive % step (mass gain in each step) and the remaining four had negative % step (mass loss in each step), the final composition of the MOR centroid after post-emplacement changes (Table 3) amounted to the gain for only two elements (+31.1% m/m for SiO_2 and +324.0% m/m for MgO) and loss for all other 8 elements (about −59.6% m/m for Na_2O to −98.8% m/m). These changes can be understood in terms of the closed, constant sum system. The chemical compositions, especially the major elements, are subjected to these constraints (e.g., Aitchison, 1986; Egozcue et al., 2003; Verma, 2020) and constitute the difficulty or impossibility in understanding the field processes from the laboratory analysis in terms of compositional measurements. In other words, the actual processes in the field (mass balance concept) cannot be recovered in the laboratory when we are dealing with closed constant sum compositional variables.

Fig. 12A shows that, even after such a large number (591) of steps of post-emplacement changes, the final altered sample still plotted in the MOR field, because, in this particular case, the discriminant functions continued to increase with the result that, after each step, the sample moved away from the dividing field boundary $B_{(MOR\text{-}OP)M}$ (Fig. 12A).

Instead of describing in detail the behaviour of the OP centroid (Table 3 and Fig. 12A), we can simply point out that the post-emplacement alteration of this sample could undergo only about 35 steps. After that, this sample moved to the MOR field (Fig. 12A). The significantly less stability of the OP centroid under the chosen step characteristics (Table 2) is due to the movement of the altered sample in each step towards the dividing field boundary $B_{(MOR\text{-}OP)M}$ (Fig. 12A). The final composition of the OP centroid after the changes accumulated in 35 steps (maximum change; the final column in Table 3) would correspond to the gain of 3 elements (about +8.8% m/m for SiO_2, +16.7% m/m for MgO, and 1.5% m/m for Na_2O) and the loss of 7 elements (from −10.2% m/m for MnO to −17.7% for K_2O).

Therefore, under the conditions listed in Table 2 for post-emplacement changes, the MOR centroid is shown to be much more stable (it remained in the MOR setting after 591 steps) than the OP centroid (it remained in the OP setting for only 35 steps). Note that we are evaluating the same steps (Table 2) for both cases (MOR and OP centroids). For other kinds of post-emplacement changes, it is quite possible that the OP centroid would be more robust than the MOR centroid.

We now briefly mention the behavior of the two centroids for the ilr_{MT} model (Fig. 12B; Table 4) from the post-emplacement steps summarized in Table 2. The MOR centroid was stable up to 511 steps, whereas the OP centroid could support only 56 steps (Fig. 12B). In the field, the mass gain or loss of the MOR centroid varied from +5766% m/m for MgO to −99% m/m for V, whereas the OP centroid showed gain or loss from +56% m/m for MgO to −43% m/m for V (Table 4). These post-emplacement changes corresponded to the values of +276% m/m for MgO to −100% m/m for V in the MOR and +27% for MgO to −54% for V (Table 4).

8.2.2. Gain or loss of one element at a time

We assumed small steps of 0.1% for gain (+0.1%) and loss (−0.1%) of one element at a time and evaluated the stability of tectonic setting of the MOR and OP centroids. The robustness of the two (MOR and OP) centroids against gain or loss of individual elements are summarized in Tables 5 and 6, for the ilr_M and ilr_{MT} models, respectively. The maximum number of steps for the gain or loss of an element at a time, for which the tectonic setting was maintained or any of the conditions of Section 5 was not violated, are listed in Tables 5 and 6. Therefore, we should examine the number of steps to know the robustness of the ilr_M (Table 5) and ilr_{MT} (Table 6) models.

Table 6
Robustness of combined major and trace element based diagram (ilr_{MT} model) against post-emplacement changes of one element at a time for step size of ±0.1% in MOR and OP centroids.

Element	Gain					Loss				
	# steps	Field (%)	Laboratory (%)		Cause for change for the next step after the # steps	# steps	Field (%)	Laboratory (%)		Cause for change for the next step after the # steps
			Evaluated element	All other elements				Evaluated element	All other elements	
MOR centroid										
SiO_2	1040	+183	+48	−48	Tectonic setting changed	842	−57	−40	+40	$(SiO_2)_{adj}$ too small
TiO_2	607	+84	+81	−1.2	Tectonic setting changed	6610	−99.9	−99.9	+1.49	$(TiO_2)_{adj}$ too small
Al_2O_3	553	+74	+57	−9.9	Tectonic setting changed	9063	−10	−10	17	$(Al_2O_3)_{adj}$ too small
$Fe_2O_3^t$	316	+37	+32	−4.1	Tectonic setting changed	8785	−10	−10	+13	$(Fe_2O_3^t)_{adj}$ too small
MnO	2191	+794	+781	−1.5	Tectonic setting changed	4535	−99	−99	+0.185	(MnO)adj too small
MgO	2276	+873	+485	−40	$(SiO_2)_{adj}$ too small	3524	−97	−97	+8	Tectonic setting changed
CaO	1913	+577	+307	−40	$(SiO_2)_{adj}$ too small	372	−31	−29	+3.71	Tectonic setting changed
Na_2O	3296	+2596	+1521	−40	$(SiO_2)_{adj}$ too small	667	−49	−48	+1.26	Tectonic setting changed
K_2O	4222	+6709	+6008	−10	Tectonic setting changed	4449	−99	−99	+0.169	$(K_2O)_{adj}$ too small
P_2O_5	5913	+36,772	+22,077	−40	$(SiO_2)_{adj}$ too small	1522	−78	−78	+0.141	Tectonic setting changed
Cr	7878	+262,722	+157,981	−40	$(SiO_2)_{adj}$ too small	4159	−98	−98	+0.0248	Tectonic setting changed
Nb	2606	+1253	+1253	−0.005	Tectonic setting changed	3774	−98	−98	+4.27	$(Nb)_{adj}$ too small
Ni	3417	+2943	+2934	−0.27	Tectonic setting changed	6837	−99.9	−99.9	+0.00934	$(Ni)_{adj}$ too small
V	1790	+498	+497	−0.16	Tectonic setting changed	8054	−10	−10	+0.0316	$(V)_{adj}$ too small
Y	8320	+408,713	+359,622	−12	Tectonic setting changed	245	−22	−22	+7.28	Tectonic setting changed
Zr	8877	+713,255	+428,883	−40	$(SiO_2)_{adj}$ too small	6831	−99.9	−99.9	+0.00928	$(Zr)_{adj}$ too small
OP centroid										
SiO_2	5250	+18907	+104	−99	$(SiO_2)_{adj}$ too large; $(MnO)_{adj}$ and $(Nb)_{adj}$ too small	799	−55	−39	+37	$(SiO_2)_{adj}$ too small
TiO_2	3521	+3276	+1974	−39	$(SiO_2)_{adj}$ too small	748	−53	−52	+1.02	Tectonic setting changed
Al_2O_3	1667	+429	+225	−39	$(SiO_2)_{adj}$ too small	682	−50	−46	+7.8	Tectonic setting changed
$Fe_2O_3^t$	1791	+499	+268	−39	$(SiO_2)_{adj}$ too small	389	−32	−29	+4.23	Tectonic setting changed
MnO	5822	+33,567	+20,594	−39	$(SiO_2)_{adj}$ too small	2700	−93	−93	+0.175	Tectonic setting changed
MgO	2213	+813	+461	−39	$(SiO_2)_{adj}$ too small	8333	−10	−10	+8.4	$(MgO)_{adj}$ too small
CaO	459	+58	+49	−6	Tectonic setting changed	8708	−10	−10	+12	$(CaO)_{adj}$ too small
Na_2O	824	+128	121	−3.1	Tectonic setting changed	7151	−99.9	−99.9	+2.56	$(Na2O)_{adj}$ too small
K_2O	4775	+11723	+7166	−39	$(SiO_2)_{adj}$ too small	5202	−99	−99	+0.53	Tectonic setting changed
P_2O_5	1879	+554	+545	−1.3	Tectonic setting changed	4797	−99	−99	+0.241	$(P_2O_5)_{adj}$ too small
Cr	5135	+16,843	+1616	−4	Tectonic setting changed	7815	−10	−10	+0.0249	$(Cr)_{adj}$ too small
Nb	10600	+3,992,183	+2,454,010	−39	$(SiO_2)_{adj}$ too small	3211	−96	−96	+0.00151	Tectonic setting changed
Ni	8598	+539,657	+331,633	−39	$(SiO_2)_{adj}$ too small	4210	−99	−99	+0.0114	Tectonic setting changed
V	7592	+197,377	+121,286	−39	$(SiO_2)_{adj}$ too small	2206	−89	−89	+0.0283	Tectonic setting changed
Y	302	+35	+35	−0.00097	Tectonic setting changed	5613	−99.6	−99.6	+0.00274	$(Y)_{adj}$ too small
Zr	8495	+486,854	+299,183	−39	$(SiO_2)_{adj}$ too small	7157	−99.9	−99.9	+0.0129	$(Zr)_{adj}$ too small

We will describe the robustness test of the gain or loss of SiO_2. For the ilr_M model, the MOR centroid was stable (maintained within the MOR field in the MOR-OP diagram) for 5141 individual steps, each of +0.1% gain of SiO_2, which means that the MOR centroid could gain +16,945% SiO_2 mass in the field, equivalent to +99% gain in the laboratory analysis (Table 5). From the mass-balance concept and constant sum of all elements to 100% in the laboratory analysis, all other major elements would show −99% loss (Table 5). The cause of change (Table 5) was that, in the next step 5142, the

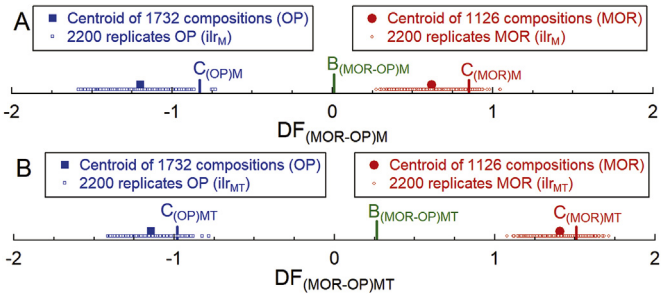

Fig. 11. One-axis multidimensional diagrams (A) $DF_{(MOR-OP)M}$ and (B) $DF_{(MOR-OP)MT}$ for the discrimination of mid-ocean ridge (MOR) and oceanic plateau (OP) settings showing the robustness of MOR and OP centroids against the analytical uncertainty propagation; centroids and boundary values are given in Fig. 2 and more details are in insets.

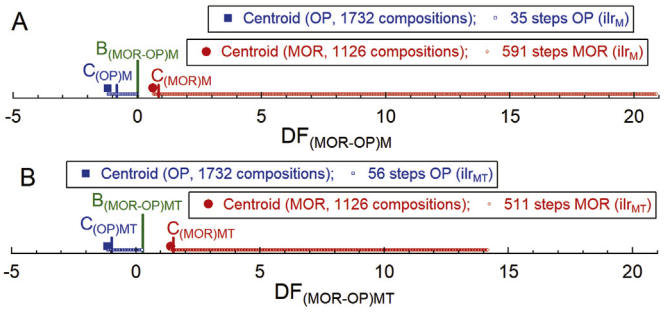

Fig. 12. One-axis multidimensional diagrams (A) $DF_{(MOR-OP)M}$ and (B) $DF_{(MOR-OP)MT}$ for the discrimination of mid-ocean ridge (MOR) and oceanic plateau (OP) settings showing the robustness of MOR and OP centroids against post-emplacement compositional changes; centroids and boundary values are given in Fig. 2 and more details are in insets.

$(SiO_2)_{adj}$ would become too large (>99%) and $(K_2O)_{adj}$ too small (<0.002%). Similarly, for the loss of −0.1% of SiO_2 in each step, the MOR centroid was stable for 105 steps, which amounted to −10% loss of SiO_2 in the field and −5.3% in the laboratory (Table 5), after which the tectonic setting would change to OP. The robustness test of the OP centroid showed 209 steps for the gain and 801 for the loss of SiO_2 (Table 5).

For the ilr_{MT} model, the MOR centroid was stable for 1040 individual steps, each of +0.1% gain of SiO_2, which means that the MOR centroid could gain +183% SiO_2 mass in the field, equivalent to +48% gain in the laboratory analysis (Table 6). The cause of change was that the tectonic setting would change to OP in the next step (1041). Similarly, for the loss of SiO_2, the maximum steps were 842 for the MOR centroid, equivalent to −57% loss of SiO_2 in the field and −40% in the laboratory (Table 6). At the next step 843, the $(SiO_2)_{adj}$ would become too small (<31%). For the OP centroid, the numbers of steps were 5250 and 799, respectively, for the gain and loss of SiO_2 (Table 6). All other "one at a time changes" are listed in Tables 5 and 6.

In summary, for the gain of an element at a time, the ilr_M model was stable for 99 steps for $Fe_2O_3^t$ to 5914 steps for P_2O_5 for the MOR centroid and for 209 steps for SiO_2 to 5824 for MnO for the OP centroid, whereas the maximum steps for the loss in the MOR centroid varied from 105 for SiO_2 to 8317 for MgO and in the OP centroid, they ranged from 197 for $Fe_2O_3^t$ to 8709 for CaO (Table 5).

For the ilr_{MT} model, the maximum number of steps for the MOR centroid varied from 316 for $Fe_2O_3^t$ to 8877 for Zr for gain and from 245 for Y to 9063 for Al_2O_3 for the loss, whereas for the OP centroid, the steps varied from 302 for Y to 10,600 for Nb for the gain and from 389 for $Fe_2O_3^t$ to 8708 for CaO (Table 6). Thus, the ilr_{MT} model seems to be more robust than the ilrM model.

9. Conclusions

Multidimensional discrimination for the mid-ocean ridge (MOR) and oceanic plateau (OP) tectonic settings was successfully achieved from 10 different models. Two of them (one based on only log-ratio transformation of all 10 major elements called ilr_M and the other from the transformation of combined 10 major and 6 trace elements called ilr_{MT}) were considered the most representative and appropriate models, which were programmed in a new software MOROPdisc for online use at the web portal http://tlaloc.ier.unam.mx. The use of higher dimensions (16 elements vs. 10 elements) provided higher success values of over 89% against 81%. MOROPdisc provides synthesis of both sample counting and probability-based counting; the latter is useful for solving the indecision of sample counting results. When complete major and trace element data are available, the ilr_{MT} model is recommended. The use of both log-ratio transformation and multi-normality renders the percent success values similar for both groups (MOR and OP).

MOROPdisc was successfully used for four test studies: (i) altered lower crustal gabbroic rocks from the Atlantis Bank, Southwest Indian Ridge, confirming the expected MOR setting; (ii) hydrothermally altered rock samples from the SW Indian Ridge close to the Rodriguez triple junction, confirming the expected MOR setting; (iii) igneous rocks from the accreted portion of the 90 Ma Colombian–Caribbean oceanic plateau, confirming the expected OP setting; and (iv) igneous rocks from the ~89–85 Ma Azuero Plateau, confirming the expected OP setting.

Two studies of ophiolites were successfully presented as application cases. Igneous rock samples from the Tertiary Mineoka ophiolite, Japan, indicated the MOR setting, whereas the igneous rock samples from the Kizildag (Hatay) ophiolite, Southern Turkey, showed more affinity with the OP setting. Two further applications presented for Precambrian rocks from West Africa and Brazil highlighted the usefulness of these multidimensional models or diagrams and confirmed the OP setting for both areas during the Precambrian.

The usefulness of the robustness module of MOROPdisc for both analytical uncertainty and post-emplacement changes was demonstrated from four examples. If the actual uncertainty values for a given sample were available, the module could evaluate the robustness from Monte Carlo simulations. For post-emplacement changes, the robustness was quantified in terms of small steps of gain or loss of all elements used in the multidimensional discrimination. The high robustness of both (ilr_M and ilr_{MT}) models were also demonstrated for the gain or loss of one element at a time. Importantly, the robustness module provides a new tool to the users to test their own samples, for which it would be advisable to estimate total uncertainties in the individual data as recently suggested and practiced by Verma et al. (2018, 2019) and Verma (2020).

Declaration of competing interest

The authors declare that they have no known competing financial interests or personal relationships that could have appeared to influence the work reported in this paper.

Acknowledgements

We are grateful to Alfredo Quiroz-Ruiz for maintaining the web portal Tlaloc and to Mauricio Rosales-Rivera for updating Tlaloc with our software MOROPdisc and the related files. We are grateful to the Editorial Advisor Prof. M. Santosh and Associate Editor Dr. Richard Palin for efficiently handling our manuscript and to two anonymous reviewers not only for their high appreciation of our work but also, more importantly, pointing out several ideas to improve our presentation.

Appendix A. Supplementary data

Supplementary data to this article can be found online at https://doi.org/10.1016/j.gsf.2020.01.005.

References

Abouchami, W., Boher, M., Michard, A., Albarede, F., 1990. A major 2.1 Ga event of mafic magmatism in West Africa: an early stage of crustal accretion. J. Geophys. Res. Solid Earth 95, 17605–17629.

Agrawal, S., 1999. Geochemical discrimination diagrams: a simple way of replacing eye-fitted boundaries with probability based classifier surfaces. J. Geol. Soc. India 54, 335–346.

Agrawal, S., Guevara, M., Verma, S.P., 2008. Tectonic discrimination of basic and ultrabasic rocks through log-transformed ratios of immobile trace elements. Int. Geol. Rev. 50, 1057–1079.

Aitchison, J., 1986. The Statistical Analysis of Compositional Data. Chapman and Hall, London, UK.

Alacali, M., Savascin, M.Y., 2015. Geothermometry and hydrothermal alteration at the Balcova geothermal field, Turkey. Geothermics 54, 136–146.

Alt, J.C., Honnorez, J., Laverne, C., Emmermann, R., 1986. Hydrothermal alteration of a 1 km section through the upper oceanic crust, Deep Sea Drilling Project hole 504B: mineralogy, chemistry, and evolution of seawater-basalt interactions. J. Geophys. Res. 91, 10309–10335.

Armstrong-Altrin, J.S., Verma, S.P., 2005. Critical evaluation of six tectonic setting discrimination diagrams using geochemical data of Neogene sediments from known tectonic settings. Sediment. Geol. 177, 115–129.

Bagci, U., Parlak, O., Höck, V., 2008. Geochemistry and tectonic environment of diverse magma generations forming the crustal units of the Kizildag (Hatay) ophiolite, southern Turkey. Turk. J. Earth Sci. 17, 43–71.

Buchs, D.M., Arculus, R.J., Baumgartner, P.O., Baumgartner-Mora, C., Ulianov, A., 2010. Late Cretaceous arc development on the SW margin of the Caribbean Plate: insights from the Golfito, Costa Rica, and Azuero, Panama, complexes. Geochemistry, Geophysics, Geosystems 11 (7). https://doi.org/10.1029/2009GC002901.

Condie, K.C., 2001. Mantle Plumes and Their Record in Earth History. Cambridge University Press, Oxford, UK, p. 306.

Egozcue, J.J., Pawlowsky-Glahn, V., Mateu-Figueras, G., Barceló-Vidal, C., 2003. Isometric logratio transformations for compositional data analysis. Math. Geol. 35, 279–300.

Furnes, H., Safonova, I., 2019. Ophiolites of the Central Asian orogenic belt: geochemical and petrological characterization and tectonic settings. Geosci. Front. 10, 1255–1284.

Hertogen, J., Emmermann, R., Robinson, P.T., Erzinger, J., 2002. Lithology, mineralogy, and geochemistry of the lower ocean crust, ODP hole735B, Southwest Indian ridge. Proc. Ocean Drill. Progr. Sci. Results 176.

Hirano, N., Ogawa, Y., Saito, K., Yoshida, T., Sato, H., Taniguchi, H., 2003. Multi-stage evolution of the Tertiary Mineoka ophiolite, Japan: new geochemical and age constraints. In: Dilek, Y., Robinson, P.T. (Eds.), Ophiolites in Earth History, vol. 218. Geological Society London Special Publication, Bath, U.K, pp. 279–298.

Humphris, S.E., Thompson, G., 1978. Hydrothermal alteration of oceanic basalts by seawater. Geochem. Cosmochim. Acta 41, 107–125.

Jochum, K.P., Verma, S.P., 1996. Extreme enrichment of Sb, Tl and other trace elements in altered MORB. Chem. Geol. 130, 289–299.

Johnston, S.T., Thorkelson, D.J., 1997. Cocos-Nazca slab window beneath Central America. Earth Planet Sci. Lett. 146, 465–474.

Kerr, A.C., Aspden, J.A., Tarney, J., Pilatasig, L.F., 2002. The nature and provenance of accreted oceanic terranes in western Ecuador: geochemical and tectonic constraints. J. Geol. Soc. Lond. 159, 577–594.

Kerr, A.C., J, T., Marriner, G.F., Nivia, A., Klaver, G.T., Saunders, A., 1996. The geochemistry and tectonic setting of late Cretaceous Caribbean and Colombian volcanism. J. S. Am. Earth Sci. 9, 111–120.

Le Roex, A.P., 1987. Source regions of mid-ocean ridge basalts: evidence for enrichment processes. In: Menzies, M., Hawkesworth, C. (Eds.), Mantle Metasomatism. Academic Press, London, pp. 389–422.

Mahoney, J.J., Jones, F.A., Frey, F.A., Salters, V.J.M., Pyle, D.G., Davies, H.L., 1995. Geochemical characteristics of lavas from Broken ridge, the Naturaliste plateau and southernmost Kerguelen plateau: Cretaceous plateau volcanism in the southeast Indian Ocean. Chem. Geol. 120, 315–345.

Marks, N., Schiffman, P., Zierenberg, R.A., Franzson, H., Fridleifsson, G.Ó., 2010. Hydrothermal alteration in the Reykjanes geothermal system: insights from Iceland deep drilling program well RN-17. Volcanol. Geotherm. Rec. 189, 172–190.

Martins, G., Oliveira, E.P., Lafon, J.-M., 2009. The Algodões amphibolite–tonalite gneiss sequence, Borborema Province, NE Brazil: geochemical and geochronological evidence for Palaeoproterozoic accretion of oceanic plateau/back-arc basalts and adakitic plutons. Gondwana Res. 15, 71–85.

Middlemost, E.A.K., 1989. Iron oxidation ratios, norms and the classification of volcanic rocks. Chem. Geol. 77, 19–26.

Morrison, D.F., 1990. Multivariate Statistical Methods, third ed. McGraw-Hill Publishing Co., New York.

Mottl, M.J., Holland, H.D., 1978. Chemical exchange during hydrothermal alteration of basalt by seawater—I. Experimental results for major and minor components of seawater. Geochem. Cosmochim. Acta 42, 1103–1115.

Nakamura, K., Kato, Y., Tamaki, K., Ishii, T., 2007. Geochemistry of hydrothermally altered basaltic rocks from the Southwest Indian ridge near the Rodriguez triple junction. Mar. Geol. 239, 125–141.

Pandarinath, K., Dulski, P., Torres-Alvarado, I.S., Verma, S.P., 2008. Element mobility during the hydrothermal alteration of rhyolitic rocks of the Los Azufres geothermal field, Mexico. Geothermics 37, 53–72.

Patten, C.G.C., Pitcairn, I.K., Teagle, D.A., Harris, M., 2016. Sulphide mineral evolution and metal mobility during alteration of the oceanic crust: insights from IODP Site 1256D. Geochem. Cosmochim. Acta 193, 132–159.

Pearce, J.A., Cann, J.R., 1971. Ophiolite origin investigated by discriminant analysis using Ti, Zr and Y. Earth Planet Sci. Lett. 12, 339–349.

Pearce, J.A., Cann, J.R., 1973. Tectonic setting of basic volcanic rocks determined using trace element analyses. Earth Planet Sci. Lett. 19, 290–300.

Rollinson, H.R., 1993. Using Geochemical Data: Evaluation, Presentation, Interpretation. Longman Scientific Technical, Essex, p. 344.

Saccani, E., 2015. A new method of discriminating different types of post-Archean ophiolitic basalts and their tectonic significance using Th-Nb and Ce-Dy-Yb systematics. Geosci. Front. 6, 481–501.

Schilling, J.-G., Zajac, M., Evans, R., Johnston, T., White, W., Devine, J.D., Kingsley, R., 1983. Petrologic and geochemical variations along the mid-Atlantic ridge from 29°N to 73°N. Am. J. Sci. 283, 510–586.

Serrano, L., Ferrari, L., López Martínez, M., Petrone, C.M., Jaramillo, C., 2011. An integrative geologic, geochronologic and geochemical study of Gorgona Island, Colombia: implications for the formation of the Caribbean large igneous province. Earth Planet Sci. Lett. 309, 324–336.

Seyfried Jr., W.E., Mottl, M.J., Bischoff, J.L., 1978. Seawater/basalt ratio effects on the chemistry and mineralogy of spilites from the ocean floor. Nature 275, 211–213.

Shervais, J.W., 1982. Ti-V plots and the petrogenesis of modern and ophiolitic lavas. Earth Planet Sci. Lett. 59, 101–118.

Smith-Duque, C.E., 2009. Hydrothermal Alteration of Upper Oceanic Crust Formed at Fast Spreading Rates. Ph.D.thesis, University of Southampton.

Staudigel, H., Hart, S.R., 1983. Alteration of basaltic glass: mechanisms and significance for the oceanic crust-seawater budget. Geochem. Cosmochim. Acta 47, 337–350.

Tejada, M.L.G., Mahoney, J.J., Neal, C.R., Duncan, R.A., Petterson, M.G., 2002. Basement geochemistry and geochronology of central Malaita, Solomon Islands, with implications for the origin and evolution of the Ontong Java Plateau. J. Petrol. 43, 449–484.

Torres-Alvarado, I.S., Pandarinath, K., Verma, S.P., Dulski, P., 2007. Mineralogical and geochemical effects due to hydrothermal alteration in the Los Azufres geothermal field, Mexico. Rev. Mex. Ciencias Geol. 24, 15–24.

Torres-Sánchez, D., Verma, S.K., Verma, S.P., Velasco-Tapia, F., Torres-Hernández, J.R., 2019. Petrogenetic and tectonic implications of Oligocene Miocene volcanic rocks from the Sierra de San Miguelito complex, central Mexico. J. S. Am. Earth Sci. 95, 102311.

Verma, S.P., 2010. Statistical evaluation of bivariate, ternary and discriminant function tectonomagmatic discrimination diagrams. Turk. J. Earth Sci. 19, 185–238.

Verma, S.P., 2012. Geochemometrics. Rev. Mex. Ciencias Geol. 29, 276–298.

Verma, S.P., 2015. Monte Carlo comparison of conventional ternary diagrams with new log-ratio bivariate diagrams and an example of tectonic discrimination. Geochem. J. 49, 393–412.

Verma, S.P., 2020. Road from Geochemistry to Geochemometrics. Springer, Singapore, ISBN 978-981-13-9277-1, p. 669.

Verma, S.P., Agrawal, S., 2011. New tectonic discrimination diagrams for basic and ultrabasic volcanic rocks through log-transformed ratios of high field strength elements and implications for petrogenetic processes. Rev. Mex. Ciencias Geol. 28, 24–44.

Verma, S.P., Armstrong-Altrin, J.S., 2013. New multi-dimensional diagrams for tectonic discrimination of siliciclastic sediments and their application to Precambrian basins. Chem. Geol. 355, 117–133.

Verma, S.P., Armstrong-Altrin, J.S., 2016. Geochemical discrimination of siliciclastic sediments from active and passive margin settings. Sediment. Geol. 332, 1–12.

Verma, S.P., Rivera-Gómez, M.A., 2013. Computer programs for the classification and nomenclature of igneous rocks. Episodes 36, 115–124.

Verma, S.P., Guevara, M., Agrawal, S., 2006. Discriminating four tectonic settings: five new geochemical diagrams for basic and ultrabasic volcanic rocks based on log-ratio transformation of major-element data. J. Earth Syst Sci. 115, 485–528.

Verma, S.P., Rivera-Gómez, M.A., Díaz-González, L., Quiroz-Ruiz, A., 2016. Log-ratio transformed major-element based multidimensional classification for altered High-Mg igneous rocks. G-cubed 17, 4955–4972.

Verma, S.P., Verma, S.K., Oliveira, E.P., 2015. Application of 55 multi-dimensional tectonomagmatic discrimination diagrams to Precambrian belts. Int. Geol. Rev. 57, 1365–1388.

Verma, S.P., Verma, S.K., Rivera-Gómez, M.A., Torres-Sánchez, D., Díaz-González, L., Amezcua-Valdez, A., Rivera-Escoto, B.A., Rosales-Rivera, M., Armstrong-Altrin, J.S., López-Loera, H., Velasco-Tapia, F., Pandarinath, K., 2018. Statistically coherent calibration of X-ray fluorescence spectrometry for major elements in rocks and minerals. J. Spectrosc. 2018, 13. https://doi.org/10.1155/2018/5837214. Article ID 5837214.

Verma, S.P., Rosales-Rivera, M., Rivera-Gómez, M.A., Verma, S.K., 2019. Comparison of matrix-effect corrections for ordinary and uncertainty weighted linear regressions and determination of major element mean concentrations and total uncertainties of sixty-two international geochemical reference materials from wavelength-dispersive X-ray fluorescence spectrometry. Spectrochimica Acta Part B: Atomic Spectroscopy 162, 105714.

Wood, D.A., 1980. The application of a Th-Hf-Ta diagram to problems of tectonomagmatic classification and to establishing the nature of crustal contamination of basaltic lavas of the British Tertiary volcanic province. Earth Planet Sci. Lett. 50, 11–30.

Yi, S.-B., Oh, C.-W., Pak, S.J., Kim, J., Moon, J.-W., 2014. Geochemistry and petrogenesis of mafic-ultramafic rocks from the Central Indian Ridge, latitude 8°–17° S: denudation of mantle harzburgites and gabbroic rocks and compositional variation of basalts. Int. Geol. Rev. 56, 691–1719.